

Rate Adaptation in Delay-Sensitive and Energy-Constrained Large-Scale IoT Networks

Mostafa Emara, *Member, IEEE*, Nour Kouzayha, *Member, IEEE*, Hesham ElSawy, *Senior Member, IEEE*, and Tareq Y. Al-Naffouri, *Senior Member, IEEE*

Abstract—Feedback transmissions are used to acknowledge correct packet reception, trigger erroneous packet re-transmissions, and adapt transmission parameters (e.g., rate and power). Despite the paramount role of feedback in establishing reliable communication links, the majority of the literature overlooks its impact by assuming genie-aided systems relying on flawless and instantaneous feedback. An idealistic feedback assumption is no longer valid for large-scale Internet of Things (IoT), which has energy-constrained devices, susceptible to interference, and serves delay-sensitive applications. Furthermore, feedback-free operation is necessitated for IoT receivers with stringent energy constraints. In this context, this paper explicitly accounts for the impact of feedback in energy-constrained and delay-sensitive large-scale IoT networks. We consider a time-slotted system with closed-loop and open-loop rate adaptation schemes, where packets are fragmented to operate at a reliable transmission rate satisfying packet delivery deadlines. In the closed-loop scheme, the delivery of each fragment is acknowledged through an error-prone feedback channel. The open-loop scheme has no feedback mechanism, and hence, a predetermined fragment repetition strategy is employed to improve transmission reliability. Using tools from stochastic geometry and queueing theory, we develop a novel spatiotemporal framework to optimize the number of fragments for both schemes and repetitions for the open-loop scheme. To this end, we quantify the impact of feedback on the network performance in terms of transmission reliability, latency, and energy consumption.

Keywords—IoT networks, Rate adaptation, Spatiotemporal analysis, Markov chains, Open-loop and closed-loop feedback.

I. INTRODUCTION

The fifth generation (5G) and beyond wireless systems are foreseen to support massive Internet of Things (IoT) deployments [1], [2]. This is evident by an unprecedented proliferation of IoT devices, which are expected to exceed 5 billion by 2025 to enable ubiquitous monitoring and smart automation of industrial systems, precision agriculture, intelligent transportation, remote healthcare, and public safety verticals [3]. Many of the emerging IoT use cases target delay-sensitive applications, where generated packets should be delivered within a predefined hard deadline [4]–[6]. Otherwise, the information within the packet becomes obsolete and is not worth transmission. For a reliable transmission that fulfills such delay constraints, rate adaptation via packet fragmentation and repetition is widely adopted in IoT technologies such

as Narrow-band IoT (NB-IoT) [7] and Long-range wide area networks (LoRaWAN) [8], [9].

In time-slotted systems, having smaller fragments implies reduced transmission rate, which in turn increases reliability of transmission per fragment¹. However, the trade-off is that smaller fragments require a larger number of successful transmissions to send a packet [10], [11]. In the presence of acknowledgment feedback, ensuring reliability and transitioning from one fragment to the next is straightforward since successfully transmitted fragments are acknowledged. However, in feedback-free scenarios, the transmitter lacks information about fragment delivery status. Consequently, it resorts to sending multiple copies of each fragment across various time slots to increase the chances of successful delivery [12], [13]. In addition to acknowledging the transmission status of fragments, feedback transmission creates an online close-loop mechanism for rate adaptation and power control [14], which is absent in the open-loop feedback-free counterpart [15], [16]. Feedback-free operation is foreseen to dominate IoT applications with stringent energy constraints. Being a major source of energy consumption, wireless transmissions should be minimized where applicable to conserve the scarce energy resource in IoT networks. In this context, eliminating the feedback transmission might be a sought solution to conserve the energy of IoT receivers, which reduces the overwhelming burden to monitor, recharge, and/or replace their batteries [17], [18]. Nevertheless, the fundamental role of feedback in wireless systems calls for innovative solutions to counter the impact of its absence, which is important to balance the trade-off between energy conservation and IoT network performance in terms of reliability and latency.

Motivated by the fundamental role of feedback on emerging delay-sensitive and energy-constrained IoT applications, this paper investigates closed-loop (i.e., feedback-assisted) and open-loop (i.e., feedback-free) rate adaptation schemes in large-scale networks. To design and assess the network key performance indicators (KPIs) of both schemes, we develop a novel spatiotemporal mathematical framework using tools from stochastic geometry and queueing theory. For the closed-loop scheme, rate adaptation is adopted based on feedback acknowledgments transmitted from the IoT receivers to their intended transmitters. In contrast to the common assumption of a perfect (lossless) delay-free feedback, we consider an error-

M. Emara, N. Kouzayha, and T. Y. Al-Naffouri are with King Abdullah University of Science and Technology, Thuwal, Saudi Arabia (e-mail: mostafa.emara@kaust.edu.sa; nour.kouzayha@kaust.edu.sa; tareq.alnaffouri@kaust.edu.sa).

H. ElSawy is with the School of Computing, Queen's University, Ontario, Canada (e-mail: hesham.elsawy@queensu.ca).

¹Instances of time-slotted multiple access are prevalent across various contemporary wireless technologies such as NB-IoT, LoRa, Sigfox, Zigbee, Bluetooth, among others. However, we maintain a general discussion to avoid diverting into intricate technology-specific nuances that might detract from the paper's focus and diminish its significance without enhancing the treatise.

prone feedback channel to investigate the negative impact of feedback impairments on transmission reliability and latency. On the other side, the open-loop scheme adopts transmitting multiple copies of each fragment aiming to increase the chance of successful delivery. Furthermore, the open-loop scheme is compared to the closed-loop benchmark. Our numerical results highlight the necessity of optimized packet fragmentation to attain a successful transmission within the predefined hard-deadline. By comparing the closed-loop and open-loop schemes, the impact of feedback presence/absence on the KPIs is revealed and quantified. Moreover, the trade-offs between transmission reliability, latency, and energy consumption are characterized.

A. Related Work

Developing mathematical frameworks to analyze the performance of large-scale time-slotted IoT networks is an attractive research topic that has been widely studied in recent years [18]–[23]. Spatiotemporal models are considered to jointly account for the massive spatial existence of IoT devices and the sporadic traffic flow per device [20], [24]–[26]. From the temporal perspective, queuing theory is utilized to conduct the microscopic analysis that accounts for the packets departure/arrival along with the devices activities. From the spatial perspective, the macroscopic analysis relies on stochastic geometry that models the aggregate interference among active devices operating on the same channel due to the shared nature of the wireless channel [19].

The recently developed spatiotemporal models have gained popularity in characterizing the transmission reliability in terms of packet successful delivery probability, latency, scalability, and stability of large-scale IoT networks [25], [27]–[32]. For instance, scalability and stability of random access in IoT networks are characterized in [25], [28]–[30]. Transmission latency of the downlink IoT network is evaluated in [31], [32]. A spatiotemporal analysis of an uplink network is conducted in [27]. However, the studies in [20], [25], [27]–[32] ignore packet latency constraints (i.e., transmission deadlines), which are critical for delay-sensitive IoT applications. The authors in [6], [33], [34] account for hard-packet deadlines while considering asynchronous periodic traffic in [33], multi-cast traffic in [34] and multi-stream traffic in [6], respectively. However, none of the spatiotemporal models in [6], [20], [25], [27]–[34] applies packet fragmentation nor time diversity (i.e., packet repetition) techniques to improve the transmission reliability.

Among the developed spatiotemporal models that characterize IoT networks, specific interest is devoted to highlighting the gains and trade-offs of the rate adaptation and repetition techniques in terms of extended coverage and increased latency. For instance, the spatiotemporal model proposed in [10] highlights the effect of static and dynamic rate adaptation in IoT networks. The works in [35], [36] characterize the delay and reliability in ultra-reliable and low-latency (URLLC) IoT networks with time diversity. However, the packet deadline constraints are ignored in [10], [35], [36]. For delay-constrained networks, frame repetition is applied in [37]–[39] to improve the successful packet delivery. However, the

analysis in [37]–[39] does not explicitly capture the temporal aspects of the traffic and KPIs.

The aforementioned spatiotemporal models assume that the feedback is lossless (perfect) and instantaneous (delay-free), which overlooks the fundamental impact of the inevitable feedback channel impairments. The work in [40] studies the impact of the erroneous feedback channel on the age of information performance for a point-to-point (i.e., not large-scale network) scenario. In fact, none of the available studies in the literature have developed a spatiotemporal analytical framework for delay-sensitive and energy-constrained large-scale IoT networks with imperfect feedback channels and open-loop/closed-loop rate adaptation (i.e., via fragmentation and repetition), which is the main focus of this paper.

B. Contributions and Organization

This article provides a novel spatiotemporal framework that utilizes stochastic geometry and queuing theory to characterize the transmission reliability, latency, and energy consumption trade-off of the open-loop rate adaptation (OLRA) and closed-loop rate adaptation (CLRA) schemes in delay-sensitive and energy-constrained large-scale IoT networks. An absorbing Markov chain (MC) is utilized to capture the temporal dimension and model the traffic flow of the IoT network with packet deadline constraint. Extensive Monte Carlo simulations are conducted to validate the accuracy of the developed analytical models. To the best of the authors' knowledge, this is the first work that provides a spatiotemporal mathematical analysis of large-scale IoT networks with rate adaptation, repetition, and feedback imperfections. The main contributions of this paper are summarized as follows.

- We develop a spatiotemporal model to characterize a feedback-free OLRA scheme with packet fragmentation and repetition to improve the likelihood of successful packet delivery. The proposed OLRA scheme is optimized and benchmarked with the CLRA scheme with packet fragmentation and feedback transmission.
- We explicitly account for feedback channel impairment in the CLRA scheme in which the receiver acknowledges the status (success or failure) of the transmitted fragments. The feedback-error-free CLRA scheme is used to benchmark the feedback-error-prone CLRA as well as the proposed OLRA schemes.
- We highlight and quantify the impact of the presence/absence of feedback and the imperfection of the feedback channel in terms of reliability, latency, and energy consumption. We also underscore the superiority of OLRA in reducing the energy consumption of IoT devices when compared to the CLRA scheme.

The rest of this paper is organized as follows. Section II introduces the system model. The CLRA and OLRA transmission schemes are defined in Section III. Section IV presents the temporal, spatial, and performance metrics analysis for the considered transmission schemes. Section V explains the numerical results. Finally, the paper is concluded in Section VI.

II. SYSTEM MODEL

A. Spatial Parameters

We focus on a pair of IoT transmitter/receiver (Tx/Rx) devices separated by a distance R_o . The impact of other coexisting IoT devices is captured via a heterogeneous Poisson field (HPF) of interferers, which is modeled by a marked Poisson process (Ψ, \mathbf{V}) . The locations of the interfering IoT devices are abstracted by a Poisson point process (PPP) Ψ of intensity λ . A set of marks $\mathbf{V} = \{1, 2, \dots, V\}$ of an arbitrary density function $f_v(v)$, independent of the devices' locations, are used to reflect the different types of the coexisting IoT devices. Each device of mark $v \in \mathbf{V}$ has a transmission power p_v and an activity factor α_v . Hence, the IoT device is active and can interfere with the intended transmission with probability α_v and is idle with probability $1 - \alpha_v$. The locations and types of the interfering devices are assumed static once realized due to the short time slot assumption that prevents tangible changes in the locations or types of devices.

Without loss of generality, a test receiver located at the origin is considered to analyze the network performance. The power-law path loss model is assumed in which the power of transmitted signals decays with the distance r at the rate $r^{-\eta}$, where $\eta > 2$ is the path-loss exponent. Moreover, the Rayleigh fading channel of unit mean power fading is considered, which is independent of different locations and types of IoT devices.

B. Temporal Parameters and Main Performance Metrics

A time-slotted system is considered with deterministic traffic arrival, where a packet is generated every T time slots. Transmitters with non-empty buffers are required to send packets of length L bits with transmission rate R_n . Hence, packets are divided into $n \leq T$ equal fragments of length $\lceil \frac{L}{nT_s} \rceil$, where the transmission and decoding of a fragment occur within a single time slot of duration T_s . The transmission rate R_n can be expressed as

$$R_n = \frac{L}{nT_s} = W \log_2(1 + \theta_n), \quad (1)$$

where W is the frequency bandwidth and $\theta_n = 2^{\frac{R_n}{W}} - 1 = 2^{\frac{L}{nWT_s}} - 1$ is the signal to interference ratio (SIR) detection threshold required to correctly decode the fragment at the intended receiver. A packet due-time of T time slots is assumed to represent hard transmission deadlines². Hence, at $t = T$, the packet is dropped from the transmitter buffer whether it is successfully delivered or not. The packet success delivery (PSD) is achieved by correctly decoding all fragments within the packet deadline T . A fragment is successfully delivered by the test receiver if the received SIR is larger than the detection threshold θ_n . Thus, the fragment success delivery (FSD) probability, denoted by p_n , is defined as $p_n = \mathbb{P}\{\text{SIR} \geq \theta_n\}$.

According to (1), dividing the packet into more fragments enhances the transmission reliability as it leads to a lower detection threshold θ_n that is more likely to be satisfied. This, however, expands the packet transmission over multiple time

slots and may increase the overall packet delivery latency. In this work, we adopt the **PSD probability** and the **PSD mean latency** as the main performance metrics to assess and compare the different proposed schemes. Moreover, the **energy consumption** of the IoT receiver during the decoding process is also considered to highlight the impact of feedback and fragment repetition on energy-constrained IoT networks.

III. TRANSMISSION SCHEMES

To enhance the PSD probability of the IoT network, we consider a fragmentation and repetition mechanism, according to which each fragment is transmitted several times. The repetition mechanism is defined based on the adopted transmission policy and whether the feedback exists or not. The CLRA is a reactive scheme, where retransmissions are triggered by a feedback signal that acknowledges the status of the fragment decoding at the receiver. In the OLRA scheme, the feedback is absent, and hence, the transmitter proactively decides on the number of repetitions to maximize the PSD probability. The transmission/decoding procedure for each scheme is detailed in the sequel.

1) Closed Loop Rate Adaptation (CLRA) Scheme: In this scheme, the intended receiver attempts to decode the transmitted fragment. In the case of successful decoding, the receiver sends an acknowledgment (ACK) message via a control channel to the transmitter to drop this fragment from its queue and send the subsequent fragment in the next time slot. Otherwise, the receiver sends a negative ACK (NACK) asking for the retransmission of the fragment. The transmitter in the NACK case keeps the same fragment at the head of its queue and persists in sending it until receiving a positive ACK from the receiver or reaching the maximum number allowed for retransmissions. An error-prone (imperfect) control channel is considered to emphasize the impact of feedback impairments on the performance metrics. Let p_{ack} denote the probability that the feedback acknowledgment (ACK/NACK) sent by the test receiver is correctly received at the paired transmitter. Similarly to the FSD, p_{ack} is the probability that the received feedback SIR is larger than an acknowledgment detection threshold θ_{ack} (i.e., $p_{\text{ack}} = \mathbb{P}\{\text{SIR}_{\text{ack}} \geq \theta_{\text{ack}}\}$). The detection threshold $\theta_{\text{ack}} = 2^{\frac{L_{\text{ack}}}{WT_{\text{ack}}}} - 1$, where L_{ack} and T_{ack} denote the acknowledgment message length and duration, respectively. Therefore, the successful delivery of a generic packet sent by R_n transmission rate from a generic IoT device is jointly controlled by the fragments and feedback successful delivery probabilities p_n and p_{ack} . The PSD and failure (time elapsed) events of the CLRA scheme are defined as follows.

Definition 1 (CLRA PSD). *A packet sent at rate R_n is successfully delivered if the receiver correctly decodes and acknowledges all the n fragments within the T time-slots period.*

Definition 2 (CLRA Packet Delivery Failure). *At any instant t , if the remaining time slots are insufficient to complete the transmission of the pending fragments related to the same packet, a CLRA failure event occurs. To save energy, a sleeping trigger signal is sent by the receiver to the transmitter to drop*

²Such assumption is convenient for time-constrained IoT applications that require *fresh* updates or measurements.

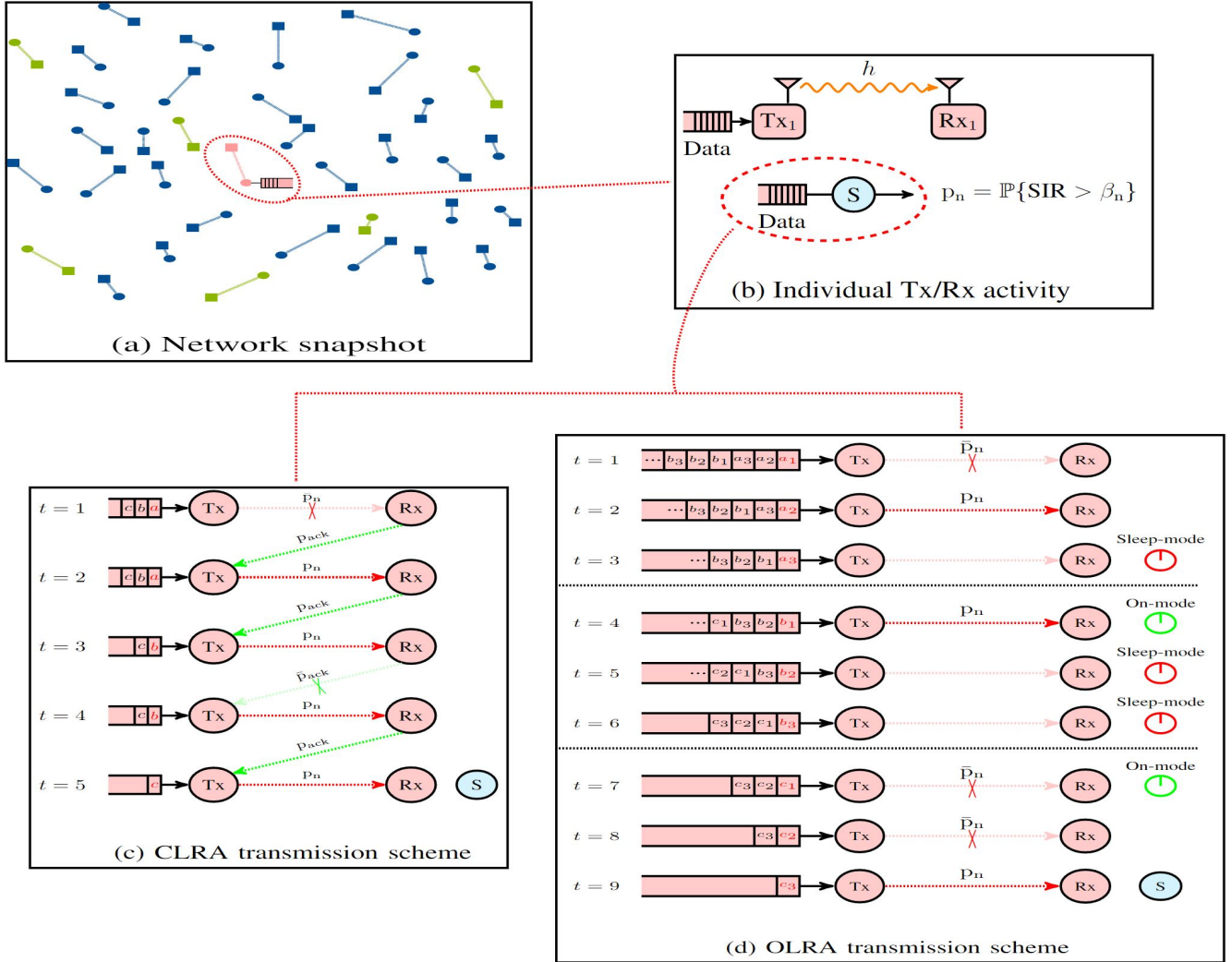


Fig. 1: (a) Snapshot of the network. Nodes, squares, and dashed lines represent transmitters, receivers, and Tx/Rx links, respectively. The test Tx/Rx is red-colored and surrounded by HPF of interferers where the active Tx/Rx links are blue-colored and inactive ones are green-colored. (b) The activity of the test Tx/Rx link. The test transmitter has a buffer for the packet fragments. The fragment is successfully delivered with probability p_n . (c) CLRA transmission scheme in the case of packet successful delivery. (d) OLRA transmission scheme in the case of packet successful delivery. Considering a packet of $n = 3$ fragments, indexed by $\{a, b, c\}$, and fragment repetition of 3 times, indexed by $\{x_1, x_2, x_3\}$ for $x \in \{a, b, c\}$.

the packet, and both of them switch to sleep mode until the next packet generation.

2) **Open Loop Rate Adaptation (OLRA) Scheme:** In this scheme, the transmitter lacks knowledge about the decoding status at the receiver, and hence, a predefined number of copies of the same fragment are transmitted to exploit temporal diversity. For the sake of maximizing the PSD, we assume that the transmitter exploits all the available T time slots for fragment repetition. This also simplifies the OLRA design as we only need to determine the optimal number of fragments n , which subsequently determines the repetition count κ . Specifically, each fragment is sent $\kappa = \lfloor T/n \rfloor$ times, where n is the total number of fragments. For the remaining $\tau = \text{mod}(T, n)$ time slots, the transmitter randomly selects $\tau < n$ fragments to be sent one more time each. Therefore, each of the selected fragments is sent $\kappa + 1$ times while the others are repeated κ

times. Note that all fragments are sent with transmission rate R_n . The PSD and failure events of the OLRA schemes can be defined as follows.

Definition 3 (OLRA PSD). A packet sent at a transmission rate R_n is successfully delivered if at least one copy of each fragment is correctly decoded within the packet deadline T .

Definition 4 (OLRA Packet Delivery Failure). In the case of decoding failure for all copies of any fragment, an OLRA failure event occurs. To save energy, the receiver stops decoding the subsequent fragments and switches to sleep mode to conserve energy. It is worth mentioning that the transmitter does not switch to sleep mode since it is unaware of the receiver status.

Fig. 1 depicts a network snapshot in which nodes represent the IoT transmitters, squares denote the receivers, and

dashed lines are for IoT Tx/Rx links. The test Tx/Rx link is represented in red color with a buffer at the test transmitter to store the packet fragments. The HPF set of interferers are blue-colored and green-colored for active and inactive Tx/Rx links, respectively. A fragment is successfully decoded with probability p_n that depends on the interference experienced at the test receiver. The first input first out (FIFO) discipline is assumed for packet service. Fig. 1 also offers a pictorial illustration of the transmission policies for CLRA and OLRA schemes in the case of packet successful delivery. The figure shows a packet of $n = 3$ fragments, indexed by $\{a,b,c\}$ and fragment repetition of 3 times, indexed by $\{x_1, x_2, x_3\}$ for $x \in \{a,b,c\}$.

The CLRA and OLRA schemes can be modeled using discrete-time absorbing Markov chains (MC) with two absorbing states, namely *success* and *timeout (failure)* states. The absorbing MC is fully characterized by the transition matrix \mathbf{P} that tracks the decoding attempts of the fragments of a packet until it is eventually absorbed to either the success or failure states. The transition matrix \mathbf{P} depends on the FSD probability p_n for the OLRA scheme and on p_n and the acknowledgment success probability p_{ack} for the CLRA scheme. We consider the different time scales of variation for the network traffic (i.e., packet generation and transmission) and channel fading when compared to the network spatial topology. In particular, the HPF of interfering devices is assumed fixed once realized, however, the channel fading and traffic vary at the scale of time slot. To account for the different IoT network realizations, we consider the meta distribution of the FSD probability. We then group the realizations that would lead to an FSD probability of a range $\pm \frac{1}{2M}$ into the same class, denoted hereafter as FSD class, where M is determined based on the needed accuracy. Thus, $p_{n,m}$ denotes the FSD probability of a fragment sent from a device that belongs to the m -th FSD class with a transmission rate R_n . On the other side, we consider averaging over all Rx/Tx links (mean-field) to find the feedback signaling success probability p_{ack} . Given $p_{n,m}$ and p_{ack} , the transition matrix $\mathbf{P}^{(m)}$ for each FSD class can be formulated for the CLRA and OLRA schemes.

IV. ANALYSIS

This section develops the mathematical frameworks to evaluate the performance of the CLRA and OLRA schemes. We start with the temporal analysis of the absorbing MC that characterizes each scheme. Hence, we construct the transition matrix $\mathbf{P}_{\text{CLRA}}^{(m)}$ for a device belonging to the m -th FSD class in terms of the successful decoding and acknowledgment probabilities $p_{n,m}$ and p_{ack} for the CLRA transmission scheme. We follow a similar approach for the OLRA scheme, where we construct the transition matrices $\mathbf{P}_{\text{OLRA}}^{(m)}$ in terms of the successful decoding probability $p_{n,m}$. Using stochastic geometry, the macroscopic network spatial analysis is handled to characterize the SIR meta distribution of the FSD for the different M classes and provide an expression for the FSD probability $p_{n,m}$, $m \in \{1, 2, \dots, M\}$ in addition to characterizing the reverse-link feedback SIR and the acknowledgment success probability p_{ack} expressions. Finally, with the aid of the matrix

analytical method (MAM) [41], the *PSD probability*, *packet delivery average latency*, and the *receiver energy consumption* are mathematically obtained.

A. Temporal Analysis

As previously mentioned, the considered schemes can be modeled by a discrete-time absorbing MC to track the fragments decoding attempts until reaching the final state where the packet is either successfully delivered or discarded due to the elapsed deadline. Consider a device belonging to the m th FSD class that transmits a packet with the rate R_n ; its corresponding MC can be mathematically represented with the transition matrix $\mathbf{P}^{(m)}$ formulated as [41, Section 3.6]

$$\mathbf{P}^{(m)} = \left[\begin{array}{c|c} \mathbf{Q}^{(m)} & \mathbf{H}^{(m)} \\ \hline \mathbf{0} & \mathbf{I} \end{array} \right] = \left[\begin{array}{c|c} \tilde{\mathbf{P}}^{(m)} & \\ \hline \mathbf{0} & \mathbf{I} \end{array} \right] = \left[\begin{array}{cccc|c} \mathbf{Q}_1^{(m)} & \mathbf{0} & \mathbf{0} & \dots & \mathbf{0} & \mathbf{H}_1^{(m)} \\ \mathbf{0} & \mathbf{Q}_2^{(m)} & \mathbf{0} & \dots & \mathbf{0} & \mathbf{H}_2^{(m)} \\ \vdots & \ddots & \ddots & \ddots & \vdots & \vdots \\ \mathbf{0} & \mathbf{0} & \mathbf{0} & \dots & \mathbf{Q}_{T-2}^{(m)} & \mathbf{H}_{T-2}^{(m)} \\ \mathbf{0} & \mathbf{0} & \mathbf{0} & \dots & \mathbf{0} & \mathbf{H}_{T-1}^{(m)} \\ \hline \mathbf{0} & \mathbf{0} & \mathbf{0} & \dots & \mathbf{0} & \mathbf{I} \end{array} \right], \quad (2)$$

where $\mathbf{Q}^{(m)}$ denotes the transient matrix describing the attempts handled by the test receiver to decode the transmitted fragments before absorption, and $\mathbf{H}^{(m)}$ denotes the absorbing matrix and captures the probability that the packet is either successfully delivered or discarded due to elapsed deadline. \mathbf{I} is an identity matrix of size 2×2 representing the success and failure absorbing states. The rows in (2) depict the progressing time evolution of the packet until absorption. The matrix $\mathbf{Q}_t^{(m)}$ represents the transition between time-slots t and $t+1$. $\mathbf{H}_t^{(m)}$ captures the absorption probability at time slot t . Next, we focus on formulating the matrix $\tilde{\mathbf{P}}^{(m)}$ presented in (2) and consisting of only $\mathbf{Q}^{(m)}$ and $\mathbf{H}^{(m)}$ for the CLRA and OLRA schemes. Without notation abuse, we drop the subscripts in $p_{n,m}$ and $\bar{p}_{n,m} = 1 - p_{n,m}$, in the hereafter matrices.

1) Temporal Analysis of the CLRA Scheme: To facilitate the exposition of the transition matrix $\tilde{\mathbf{P}}_{\text{CLRA}}^{(m)}$ of the CLRA scheme, we first present an illustrative example for the transmission of a packet with $n = 3$ fragments and packet due-time $T = 8$ time slots. We then generalize $\tilde{\mathbf{P}}_{\text{CLRA}}^{(m)}$ for different transmission rates and due-times. Fig. 2 depicts the absorbing MC of the considered illustrative example. The three fragments of the packet are denoted as $\{a, b, c\}$ and are retransmitted several times according to the feedback of the receiver. Fig. 2 starts with an idle state to represent the empty buffer at the test transmitter at instant $t = 0$. At $t = 1$, fragment a is sent, and its first decoding attempt is handled at the test receiver. This is represented by a transition with probability 1 between time slots $t = 0$ and $t = 1$. The successful delivery of a packet's fragment sent from an m -FSD class IoT device with a transmission rate R_n is conditioned on the joint successful decoding at the test receiver (of probability $p_{n,m}$) and successful acknowledgment (of probability p_{ack}). Thus,

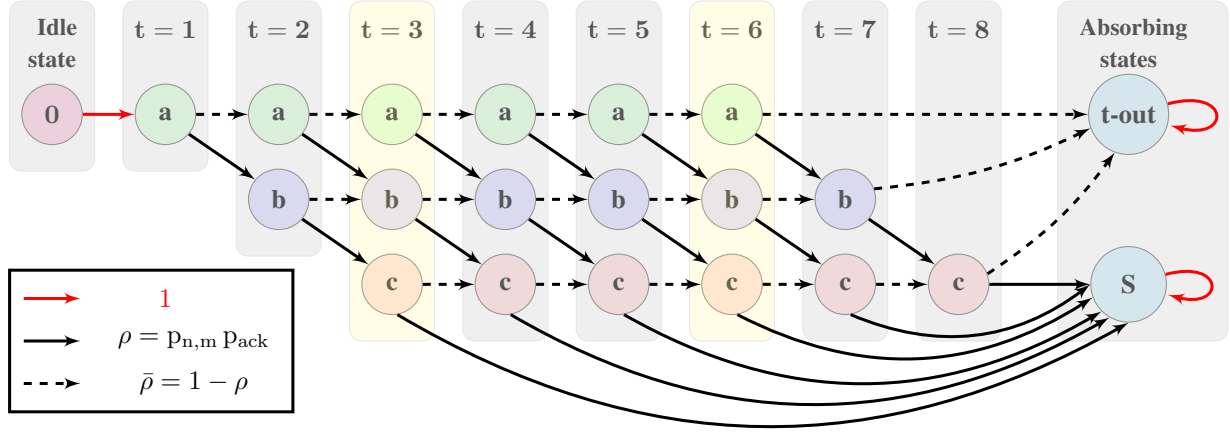


Fig. 2: The absorbing MC of the CLRA scheme. The packet consists of $n = 3$ fragments, denoted by $\{a,b,c\}$, and the packet deadline $T = 8$.

the fragment success delivery probability of the CLRA scheme is $\rho = p_{n,m} P_{\text{pack}}$. If fragment a is successfully delivered (i.e., jointly decoded and acknowledged) of probability ρ , the transmitter drops it from the queue and switches to transmit fragment b in the next time slot. Otherwise, the transmitter persists in sending fragment a during the subsequent time slots. The retransmission/decoding trials of fragment a proceed until it is successfully delivered or the maximum number of retransmissions is reached. If the later event happens, the packet is discarded. Note that a packet is discarded at instant t if the remaining $(T - t)$ time slots are insufficient to transmit all the pending fragments related to the same packet. When this happens, both transmitter and receiver switch to sleeping mode until the next packet generation. The same strategy is followed for the other fragments until the CLRA PSD event, defined in Definition 1, occurs. According to this policy, the instant $t = 2$ carries either the 2nd trial to deliver fragment a after a single failure (due to either decoding failure or corrupted/lost ACK) or the 1st attempt to deliver fragment b after the successful delivery of fragment a . Then, $t = 3$ can have one of the following 4 possibilities; (i) the 3rd trial to deliver fragment a after two consecutive failures; (ii) the 1st trial to deliver fragment b after one failure followed by a single success in delivering fragment a ; (iii) the 2nd delivering attempt of fragment b after the successful delivery of fragment a followed by a failure of delivering fragment b ; and (iv) the 1st trial to deliver fragment c after two consecutive successful delivering attempts for fragments a and b .

By construction, at least n time slots are required for the CLRA packet delivery event to succeed. This is visualized in Fig. 2 by following the best-case scenario represented by the diagonal transitions from a to b then c , where the success event occurs, at $t = 3$. On the other side, the packet discarding event is due to successive failures in delivering the transmitted fragments. This is also manifested in Fig. 2 by the absorption into the timeout state, for example, at $t = 6$ after 6 successive delivering failures of fragment a . The detailed structure of the transition matrix $\tilde{P}_{\text{CLRA}}^{(m)}$ for the absorbing

$$\tilde{P}_{\text{CLRA}}^{(m)} = \left[\begin{array}{c|c} \mathbf{Q}_{\text{CLRA}}^{(m)} & \mathbf{H}_{\text{CLRA}}^{(m)} \end{array} \right]$$

$$= \begin{array}{c|cccccccc|cc} & a & b & a & b & c & a & b & c & a & b & c & b & c & c & S & t\text{-out} \\ \hline t = 1 & a & \bar{\rho} & \rho & & & & & & & & & & & & & \\ & b & & & & & & & & & & & & & & & \\ \hline t = 2 & a & & & & & & & & & & & & & & & \\ & b & \bar{\rho} & \rho & 0 & & & & & & & & & & & & \\ & c & 0 & \bar{\rho} & \rho & & & & & & & & & & & & \\ \hline t = 3 & a & & & & & & & & & & & & & & 0 & 0 \\ & b & & & & & & & & & & & & & & 0 & 0 \\ & c & & & & & \bar{\rho} & \rho & 0 & & & & & & & \rho & 0 \\ & & & & & & 0 & \bar{\rho} & \rho & & & & & & & 0 & 0 \\ \hline t = 4 & a & & & & & & & & & & & & & & 0 & 0 \\ & b & & & & & & & & & & & & & & 0 & 0 \\ & c & & & & & & & & & & & & & & \rho & 0 \\ & & & & & & & & & & & & & & & 0 & 0 \\ \hline t = 5 & a & & & & & & & & & & & & & & 0 & 0 \\ & b & & & & & & & & & & & & & & 0 & 0 \\ & c & & & & & & & & & & & & & & \rho & 0 \\ & & & & & & & & & & & & & & & 0 & 0 \\ \hline t = 6 & a & & & & & & & & & & & & & & 0 & \bar{\rho} \\ & b & & & & & & & & & & & & & & 0 & 0 \\ & c & & & & & & & & & & & & & & \rho & 0 \\ & & & & & & & & & & & & & & & 0 & \bar{\rho} \\ \hline t = 7 & b & & & & & & & & & & & & & & \rho & \bar{\rho} \\ & c & & & & & & & & & & & & & & \rho & 0 \\ & & & & & & & & & & & & & & & 0 & \bar{\rho} \\ \hline t = 8 & c & & & & & & & & & & & & & & 0 & \rho & \bar{\rho} \end{array} \quad (3)$$

MC in Fig. 2 is given by (3). The structure of $\tilde{P}_{\text{CLRA}}^{(m)}$ in (3) follows the general transition matrix structure in (2). The transient matrix $\mathbf{Q}_{\text{CLRA}}^{(m)}$ consists of the non-zero diagonal submatrices $\mathbf{Q}_t^{(m)}$, $t = \{1, 2, \dots, T-2\}$ and zero submatrices of appropriate sizes, which are left blanked. For $1 \leq t < n$, it can be noticed that $\mathbf{Q}_t^{(m)}$ is a fat matrix of dimension $t \times (t+1)$. Thus, its size gradually grows with time evolution. For $n \leq t < T-n+1$, $\mathbf{Q}_t^{(m)}$ is a square matrix with unchanged dimension of $n \times n$. Finally, for $T-n+1 \leq t \leq T-2$, $\mathbf{Q}_t^{(m)}$ is a thin matrix of dimension $(T-t+1) \times (T-t)$, hence it gradually declines with time progress. We denote by $\mathbf{Q}\mathbf{Q}_t^{(m)}$, $\mathbf{Q}\mathbf{U}_t^{(m)}$ and $\mathbf{Q}\mathbf{D}_t^{(m)}$ the fat, square and thin $\mathbf{Q}_t^{(m)}$ matrices in the three mentioned time intervals. On the other hand, the absorbing matrix $\mathbf{H}_{\text{CLRA}}^{(m)}$ consists of two-column submatrices $\mathbf{H}_t^{(m)}$, $t = \{1, 2, \dots, T-1\}$ to capture the packet absorption into the success and failure absorbing states. It can be shown that the first possibility for a packet to be absorbed into the success state occurs at $t = n$ and into the timeout state at $t = T - n + 1$, which complies with Fig. 2. The transition matrix $\tilde{P}_{\text{CLRA}}^{(m)}$ in (3) describing the absorbing MC

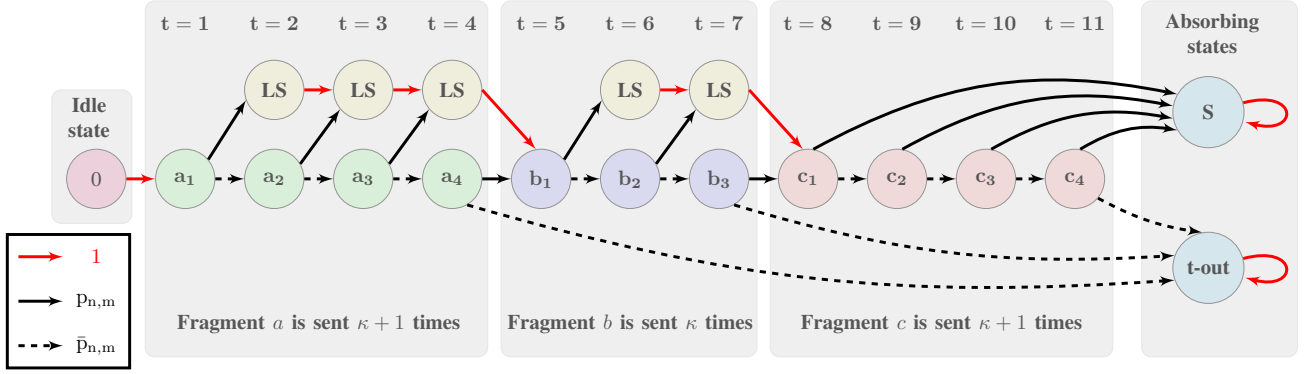


Fig. 3: The absorbing MC of the OLRA scheme. The packet consists of $n = 3$ fragments, denoted as $\{a, b, c\}$ and the packet deadline $T = 11$. So, $\kappa = \lfloor T/n \rfloor = 3$, and $\tau = \text{mod}(T, n) = 2$. Hence, each fragment is sent κ times while $\tau = 2$ fragments are randomly chosen to be sent one more time. We assume that $\{a, c\}$ are the selected fragments. The subscript in $x_i, x \in \{a, b, c\}$ denotes the i th decoding attempt.

of the CLRA scheme for $n = 3$ fragments and packet due-time $T = 8$. Lemma 1 provides the general CLRA transition matrix $\tilde{P}_{\text{CLRA}}^{(m)}$ for arbitrary tuple (n, T) .

Lemma 1 (CLRA Transition Matrix). The transition matrix $\tilde{P}_{\text{CLRA}}^{(m)}$ describing the absorbing MC for a generic packet sent from an m -FSD class IoT device consists of the submatrices $Q_t^{(m)}$ and $H_t^{(m)}$ for an arbitrary tuple (n, T) , which are given by (4) and (5), respectively. $X \Big|_{i \times j}$ denotes a matrix X of size $(i \times j)$ and the notations $\{G, U, D\}$ in $\{QG_t^{(m)}, QU_t^{(m)}, QD_t^{(m)}\}$ and $\{HU_t^{(m)}, HD_t^{(m)}\}$ refer to {growing, unchanged, and declining}-size matrices, respectively.

$$Q_t^{(m)} = \begin{cases} QG_t^{(m)} \Big|_{t \times (t+1)} & 1 \leq t < n, \\ QU_t^{(m)} \Big|_{n \times n} & n \leq t < T - n + 1, \\ QD_t^{(m)} \Big|_{(T-t+1) \times (T-t)} & T - n + 1 \leq t \leq T - 2, \end{cases} \quad (4)$$

$$H_t^{(m)} = \begin{cases} 0 \Big|_{t \times 2} & 1 \leq t < n, \\ HU_t^{(m)} \Big|_{n \times 2} & n \leq t < T - n + 1, \\ HD_t^{(m)} \Big|_{(T-t+1) \times 2} & T - n + 1 \leq t \leq T - 2, \\ \begin{bmatrix} \rho & \bar{\rho} \end{bmatrix} & t = T - 1, \end{cases} \quad (5)$$

where the elements of the matrices $QG_t^{(m)}$, $QU_t^{(m)}$ and $QD_t^{(m)}$ in (4) are given by

$$QG_t^{(m)}(i, j) = QU_t^{(m)}(i, j) = \begin{cases} \bar{\rho}, & \text{for } j = i, \\ \rho, & \text{for } j = i + 1, \\ 0, & \text{otherwise,} \end{cases}$$

$$QD_t^{(m)}(i, j) = \begin{cases} \rho, & \text{for } i = j, \\ \bar{\rho}, & \text{for } i = j + 1, \\ 0, & \text{otherwise.} \end{cases} \quad (6)$$

and the elements of $HU_t^{(m)}$ and $HD_t^{(m)}$ in (5) are given by

$$HU_t^{(m)}(i, j) = \begin{cases} \rho, & \text{for } i = n, j = 1 \\ 0, & \text{otherwise,} \end{cases}$$

$$HD_t^{(m)}(i, j) = \begin{cases} \rho, & \text{for } i = 1, j = 2 \\ \bar{\rho}, & \text{for } i = T - t + 1, j = 1 \\ 0, & \text{otherwise.} \end{cases} \quad (7)$$

2) Temporal Analysis of the OLRA Scheme: The OLRA scheme implements proactive packet repetition with rate adaptation to improve the transmission reliability of feedback-free IoT networks. In this scheme, the packet is divided into n fragments and transmitted with the rate R_n several times. In particular, given that $\kappa = \lfloor \frac{T}{n} \rfloor$ and $\tau = \text{mod}(T, n)$, each fragment is sent κ times while the remaining τ time slots are exploited to transmit each of the randomly selected $\tau < n$ fragments one more time. In other words, the i th fragment is sent $\epsilon_i = \kappa + \mathbb{1}_i$, $i \in \{1, 2, \dots, n\}$ times, where $\mathbb{1}_i$ is an indicator function which is equal to 1 if the fragment is sent $(\kappa + 1)$ times of probability $\frac{\tau}{n}$ and 0 if the fragment is sent κ times of probability $(1 - \frac{\tau}{n})$. Consequently, the test receiver has ϵ_i possible decoding chances for the i th fragment.

Fig. 3 shows the absorbing MC of the OLRA scheme for a given tuple $(n = 3, T = 11)$, therefore $\tau = 2$ and $\kappa = 3$. For illustration, the figure assumes that fragments $\{a, c\}$ are selected to be sent $\kappa + 1 = 4$ times while fragment b is sent $\kappa = 3$ times. The subscript i in a_i denotes the i -th transmission/decoding attempt of fragment a . As shown in Fig. 3, the PSD is conditioned by the successful decoding of all the n fragments. For the i th fragment, if all the ϵ_i decoding attempts fail, the packet is discarded, and the receiver goes into sleeping mode until the reception of the next packet. In contrast, if any decoding attempt of a fragment, except the last fragment, succeeded, the receiver has to wait until receiving the subsequent fragment and follow the same procedure. This waiting is represented by a transition into a success logic state (LS), which records the required FSD event. For the last fragment, the successful decoding of any attempts directly leads to packet absorption into the success state. Fig. 3 reveals that, in the OLRA scheme, a similar pattern exists for all

fragments, except for the last fragment, which should be reflected in the structure of the transition matrix $\mathbf{P}_{\text{OLRA}}^{(m)}$ that characterizes the absorbing MC. Thus, the transition matrix $\mathbf{P}_{\text{OLRA}}^{(m)}$ of the OLRA scheme in Fig. 3 is given by (8), where LS in the columns and rows labels denotes the success logic state shown in Fig. 3. The transition matrix $\tilde{\mathbf{P}}_{\text{OLRA}}^{(m)}$ in (8) shows similar transient and absorbing matrices for fragments a and b that differ from those of fragment c . The dashed horizontal lines separate the $\epsilon_i, \forall i$ submatrices that track the decoding trials of the i^{th} fragment.

$$\tilde{\mathbf{P}}_{\text{OLRA}}^{(m)} = \left[\mathbf{Q}_{\text{OLRA}}^{(m)} \mid \mathbf{H}_{\text{OLRA}}^{(m)} \right] =$$

	a_2	LS	a_3	LS	a_4	LS	b_1	b_2	LS	b_3	LS	c_1	c_2	c_3	c_4	S	t-out
$t = 1$	a_1	\bar{p}	p														
$t = 2$	a_2		\bar{p}	p													
$t = 3$	a_3			\bar{p}	p												
$t = 4$	a_4					p										0	\bar{p}
$t = 5$	b_1						\bar{p}	p								0	0
$t = 6$	b_2							\bar{p}	p								
$t = 7$	b_3									p						0	\bar{p}
$t = 8$	c_1										\bar{p}					p	0
$t = 9$	c_2											\bar{p}				p	0
$t = 10$	c_3												\bar{p}			p	0
$t = 11$	c_4													0		p	\bar{p}

The following lemma provides the general OLRA transition matrix $\tilde{\mathbf{P}}_{\text{OLRA}}^{(m)}$ for arbitrary tuple (n, T) .

Lemma 2 (OLRA Transition Matrix). The transition matrix $\tilde{\mathbf{P}}_{\text{OLRA}}^{(m)}$ describing the absorbing MC for a generic packet sent from an m -FSD class IoT device consists of the submatrices $\mathbf{Q}_{t,\text{OLRA}}^{(m)}$ and $\mathbf{H}_{t,\text{OLRA}}^{(m)}$ for an arbitrary tuple (n, T) , which are given by

$$\tilde{\mathbf{P}}_{\text{OLRA}}^{(m)} = \left[\mathbf{Q}_{\text{OLRA}}^{(m)} \mid \mathbf{H}_{\text{OLRA}}^{(m)} \right]$$

$$= \begin{bmatrix} \mathbf{Q}_1^{(m)} & & & & & & \mathbf{H}_1^{(m)} \\ & \mathbf{Q}_2^{(m)} & & & & & \mathbf{H}_2^{(m)} \\ & & \ddots & & & & \vdots \\ & & & \mathbf{Q}_n^{(m)} & & & \mathbf{H}_n^{(m)} \end{bmatrix} \quad (9)$$

where

$$\mathbf{Q}_i^{(m)} = \begin{bmatrix} \mathbf{Q}_{i,1} & & & & \\ & \mathbf{Q}_{i,2} & & & \\ & & \ddots & & \\ & & & \mathbf{Q}_{i,\epsilon_i} & \end{bmatrix}, \quad i \in \{1, 2, \dots, n-1\}$$

$$\mathbf{Q}_{i,1} = \begin{bmatrix} \bar{p} & p \\ 0 & 1 \end{bmatrix}, \quad \mathbf{Q}_{i,2 \leq k \leq \epsilon_i - 1} = \begin{bmatrix} \bar{p} & p \\ 0 & 1 \end{bmatrix},$$

$$\mathbf{Q}_{i,\epsilon_i} = \begin{bmatrix} p \\ 1 \end{bmatrix}, \quad \mathbf{Q}_n^{(m)} = \bar{p} \mathbf{I}_{\epsilon_n - 1} \quad (10)$$

and

$$\mathbf{H}_i^{(m)} = \begin{bmatrix} \mathbf{H}_{i,1} \\ \mathbf{H}_{i,1} \\ \vdots \\ \mathbf{H}_{i,\epsilon_i} \end{bmatrix}, \quad i \in \{1, 2, \dots, n-1\}$$

$$\mathbf{H}_{i,1} = \mathbf{0}_{1 \times 2}, \quad \mathbf{H}_{i,2 \leq k \leq \epsilon_i - 1} = \mathbf{0}_{2 \times 2}, \quad \mathbf{H}_{i,\epsilon_i} = \begin{bmatrix} 0 & \bar{p} \\ 0 & 0 \end{bmatrix},$$

$$\mathbf{H}_{n,1 \leq k \leq \epsilon_n - 1} = [p \ 0], \quad \mathbf{H}_{n,\epsilon_n} = [p \ \bar{p}], \quad (11)$$

Remark 1. For the sake of energy saving, another variant of the OLRA scheme is suggested. In this scheme, each fragment is sent $\kappa = \lfloor T/n \rfloor$ times, and the remaining $\tau = \text{mod}(T, n)$ time slots are kept silent. We denote this scheme as **OLRA with energy saving (OLRA-ES)**. The transition matrix $\tilde{\mathbf{P}}_{\text{OLRA-ES}}^{(m)}$ of the OLRA-ES scheme is similar to the transition matrix of the OLRA scheme given in (9) with $\epsilon_i = \kappa$ instead of $\kappa + \mathbb{1}_i$ for fragments $i \in \{1, 2, \dots, n\}$.

B. Spatial Analysis

In this subsection, the network-wide spatial analysis is conducted using stochastic geometry to characterize the FSD probability for a generic m -FSD device $p_{n,m}$ and the feedback success probability p_{ack} that controls the transition matrices given in Lemmas 1 and 2.

1) Forward Fragment Success Delivery Probability:

Thanks to the independent thinning property of the PPP, the set of IoT devices of type $v \in \mathbf{V}$ is an independent PPP denoted by $\Psi_v \subset \Psi$ with intensity $\lambda_v = f_v(v)\lambda$. The FSD probability is defined as the probability that the received signal at the test receiver located at the origin is larger than the SIR detection threshold θ_n when the packet is transmitted with the rate R_n . Therefore, p_n can be expressed as

$$p_n = \mathbb{P} \{ \text{SIR} \geq \theta_n \mid \Psi \}$$

$$= \mathbb{P} \left\{ \frac{p_o h_o \|x_o\|^{-\eta}}{\sum_{v=1}^V \sum_{x_i \in \Psi_v \setminus x_o} \mathbb{1}_{\xi_i} p_v h_i \|x_i\|^{-\eta}} \geq \theta_n \mid \Psi \right\}, \quad (12)$$

where p_o is the power of the intended signal, h_o is the desired channel gain, $\|x_o\|$ is the distance between the test receiver at the origin and its test transmitter, $x_i \in \Psi_v$ is the location of an interfering IoT device of type v , h_i is the interfering channel gain, $\mathbb{1}_{\xi_i}$ is an indicator function which is equal to one if the x_i interfering IoT device is active and equal zero otherwise, and $\|x_i\|$ is the distance between the i -th interfering device and the test receiver. For an arbitrary realization of the HPF, the FSD p_n is a function of the locations of the interfering devices. Such realization-dependent FSD is fully characterized via the meta distribution of the FSD probability, which is defined as

$$\bar{F}_s(\theta_n, \delta) = \mathbb{P} \{ \mathbb{P} \{ \text{SIR} \geq \theta_n \mid \Psi \} > \delta \} = \mathbb{P} \{ p_n > \delta \}. \quad (13)$$

$\bar{F}_s(\theta_n, \delta)$ defines the likelihood that the decoding process at the test receiver within an arbitrary realization of the HPF, with a detection threshold θ_n , succeeds for more than δ percent of the time. Thus, for a given set of parameters n and δ , (13) generalizes the FSD model for all realizations of the

HPF. For analytical tractability, the meta distribution in (13) is approximated using the beta approximation as follows [42]

$$\bar{F}_s(\theta_n, \delta) \approx 1 - \mathcal{I}_\delta(M_1 \mathcal{X}, (1 - M_1) \mathcal{X}), \quad (14)$$

where M_1 and M_2 are the first two moments of the FSD probability at rate R_n , $\mathcal{X} = (M_1 - M_2)/(M_2 - M_1^2)$, $\mathcal{I}_\delta(a, b) = \frac{1}{\mathcal{B}(a, b)} \int_0^\delta t^{a-1} (1-t)^{b-1} dt$ is the regularized incomplete beta function, and $\mathcal{B}(x, y) = \int_0^\infty \frac{t^{x-1}}{(1+t)^{x+y}} dt$ is the beta function. The moments M_1 and M_2 of the FSD probability are given as in the following lemma.

Lemma 3 (Moments of FSD probability). The moments M_1 and M_2 of the FSD probability p_n are given as

$$M_1 = \exp \left[\frac{-2\pi^2 R_o^2 \theta_n^{\frac{2}{\eta}}}{\eta \sin \left(\frac{2\pi}{\eta} \right)} \sum_{v=1}^V \left(\frac{p_v}{p_o} \right)^{\frac{2}{\eta}} \lambda_v \alpha_v \right], \quad (15)$$

$$M_2 = \exp \left[\frac{-2\pi^2 R_o^2 \theta_n^{\frac{2}{\eta}}}{\eta \sin \left(\frac{2\pi}{\eta} \right)} \sum_{v=1}^V \left(\frac{p_v}{p_o} \right)^{\frac{2}{\eta}} \lambda_v \alpha_v \left(2 - \alpha_v \left(1 - \frac{2}{\eta} \right) \right) \right]. \quad (16)$$

Proof: See Appendix A. ■

To conduct the queuing analysis, the approximated meta distribution in (14) is discretized into M equiprobable FSD classes. To define the FSD probability ranges for the different classes, we set $w_0 = 0$ and $w_M = 1$, and define the set $\{w_2, w_3, \dots, w_{M-1}\}$ such that

$$\bar{F}_s(\theta_n, w_m) - \bar{F}_s(\theta_n, w_{m-1}) = \frac{1}{M}. \quad (17)$$

The FSD probabilities within the range $[w_m, w_{m+1}]$ are approximated via the median value $p_{n,m}$, which is given by

$$\bar{F}_s(\theta_n, w_m) - \bar{F}_s(\theta_n, p_{n,m}) = \frac{1}{2M}. \quad (18)$$

The above discretization implies that the likelihood for the intended IoT link to operate with any of the FSD probabilities $p_{n,m}$ is $\frac{1}{M}$. Using the discretized $p_{n,m}$, we can build a queuing model for each FSD class for the CLRA and OLRA schemes as shown in Section IV-A.

2) **Feedback Success Probability:** The feedback success probability p_{ack} is defined as the probability that the feedback SIR is larger than a detection threshold θ_{ack} . Assuming that the typical transmitter x_o , located at the origin, receives a feedback message (i.e., either ACK or NACK) from its corresponding receiver y_o , the feedback success probability is given as

$$\begin{aligned} p_{\text{ack}} &= \mathbb{P} \{ \text{SIR}_{\text{ack}} \geq \theta_{\text{ack}} \} \\ &= \mathbb{P} \left\{ \frac{p_t h_o \|y_o - x_o\|^{-\eta}}{\sum_{y_i \in \Psi \setminus y_o} p_t h_i \|y_i - x_o\|^{-\eta}} \geq \theta_{\text{ack}} \right\} \end{aligned} \quad (19)$$

where p_t is the feedback transmit power. We assume that all interfering IoT receivers $y_i \in \Psi$ have the same feedback transmit power p_t . The feedback success probability p_{ack} is given by the following Lemma.

Lemma 4 (Feedback success probability). The feedback success probability defined in (19) is given as

$$p_{\text{ack}} = \exp \left[\frac{-2\pi^2 \lambda R_o^2 \theta_{\text{ack}}^{\frac{2}{\eta}}}{\eta \sin \left(\frac{2\pi}{\eta} \right)} \right] \quad (20)$$

Proof: The proof follows a similar approach as in Lemma 3, thus omitted. ■

C. Performance Metric Analysis

In this section, the main performance metrics of the CLRA and OLRA schemes are formulated given the transition matrices provided in Lemmas 1 and 2. By referring to the MAM, the PSD probability and mean latency for a device in the m -th FSD class are expressed in Theorem 1.

Theorem 1. Let the vector $\mathbf{A}^{(m)} \in \{A_s^{(m)}, A_f^{(m)}\}$ defines the probability that a generic packet of a device that belongs to the m -th FSD class is eventually absorbed into the success or timeout (failure) states, respectively, where $A_f^{(m)} = 1 - A_s^{(m)}$. In addition, let $\mathbf{D}^{(m)} \in \{D_s^{(m)}, D_f^{(m)}\}$ denotes a scaled mean latency (delay) to absorption for a device in the m -th FSD class, where $\frac{D_s^{(m)}}{A_s^{(m)}}$ and $\frac{D_f^{(m)}}{A_f^{(m)}}$ are, respectively, the packet mean latency, in time slots, for absorption into success and timeout states. Thus, $\mathbf{A}^{(m)}$ and $\mathbf{D}^{(m)}$ can be defined as [41]

$$\mathbf{A}^{(m)} = \mathbf{H}_1^{(m)} + \sum_{i=2}^{T-2} \left(\prod_{t=1}^{i-1} \mathbf{Q}_t^{(m)} \right) \times \mathbf{H}_i^{(m)}. \quad (21)$$

$$\mathbf{D}^{(m)} = \mathbf{H}_1^{(m)} + \sum_{i=2}^{T-2} \left(\prod_{t=1}^{i-1} i \mathbf{Q}_t^{(m)} \right) \times \mathbf{H}_i^{(m)}. \quad (22)$$

Proof: According to (2), the transition probability within the decoding attempts before the absorption into a final state is captured by the transient matrix $\mathbf{Q}^{(m)}$ and the probability of absorption is captured by $\mathbf{H}^{(m)}$. Hence, the probability that the receiver handles t consecutive decoding attempts is given by $\prod_{i=1}^t \mathbf{Q}_i^{(m)}$. Similarly, the probability that a generic packet is absorbed after exactly t time slots is given by $\prod_{i=1}^{t-1} \mathbf{Q}_i^{(m)} \mathbf{H}_t^{(m)}$. Therefore, by applying the law of total probability and accounting for the T -time slot packet deadline, Theorem 1 is proved. ■

Note that $\mathbf{D}^{(m)}$ in (22) determines the average number of time slots for packet absorption into success or timeout states. The mean packet round-trip latency depends on the adopted transmission strategy. Therefore, the mean packet latency for the CLRA and OLRA schemes is given in Corollary 1.

Corollary 1. The mean absorption (to transmission success or elapsed deadline) latency of a generic packet for a device belonging to the m -FSD class for the CLRA scheme is given as

$$\mathbf{D}_{\text{CLRA}}^{(m)} = \mathbf{D}^{(m)} (T_s + T_{\text{ack}}) \text{ sec}, \quad (23)$$

and for the OLRA scheme, the mean absorption latency is given as

$$\mathbf{D}_{\text{OLRA}}^{(m)} = \mathbf{D}^{(m)} T_s \text{ sec}, \quad (24)$$

where T_{ack} is the feedback message duration, which is significantly shorter than the fragment duration T_s owing to the short ACK/NACK messages.

The overall energy consumption of a generic test receiver that belongs to the m -FSD class depends on the adopted transmission policy. In the OLRA scheme, the test receiver consumes energy in packet fragment reception and decoding. In the CLRA scheme, the receiver consumes extra energy in feedback ACK/NACK signaling transmission. The energy consumptions of the test receiver in the fragment reception and decoding and the feedback acknowledgment denoted as E_r and E_{ack} , are given as [43], [44]

$$\begin{aligned} E_r &= p_{cr} T_s, \\ E_{\text{ack}} &= (\gamma p_t + p_{ct}) T_{\text{ack}}, \end{aligned} \quad (25)$$

where p_{cr} is the radio frequency (RF) circuit power consumption at the receiver, p_{ct} denotes the RF circuit power consumption of the test receiver's transceiver in transmitting the ACK/NACK feedback messages, p_t is the feedback transmitted power, and γ is the power amplifier conversion factor of value at least 1.

Finally, the total energy consumption during packet delivery depends on the mean latency for packet absorption, whether to success or time-out states. The total energy consumption of a receiver belonging to the m -FSD class is given by the following corollary.

Corollary 2. The overall energy consumption of an m -FSD class device for the CLRA and OLRA transmission schemes is given by

$$\begin{aligned} E_{\text{CLRA}}^{(m)} &= (E_r + E_{\text{ack}}) (D_{s,\text{CLRA}}^{(m)} + D_{f,\text{CLRA}}^{(m)}), \\ E_{\text{OLRA}}^{(m)} &= E_r (D_{s,\text{OLRA}}^{(m)} + D_{f,\text{OLRA}}^{(m)}), \end{aligned}$$

Finally, by averaging over the FSD classes, the probability that a packet is absorbed to either success or failure states, \mathbf{A} , the mean latency for such absorption \mathbf{D} , and the energy consumption at the test IoT receiver are given as

$$\begin{aligned} \mathbf{A} &= \mathbb{E}_m \left\{ \mathbf{A}^{(m)} \right\} \\ \mathbf{D}_x &= \mathbb{E}_m \left\{ \mathbf{D}_x^{(m)} \right\} \\ \mathbf{E}_x &= \mathbb{E}_m \left\{ \mathbf{E}_x^{(m)} \right\} \end{aligned} \quad (26)$$

where $x \in \{\text{CLRA}, \text{OLRA}\}$.

V. NUMERICAL RESULTS

In this section, we provide numerical results to highlight the impact of the repetition mechanism and the feedback presence/absence on the developed CLRA and OLRA schemes. Monte Carlo simulations are carried out to validate the accuracy of the developed analytical models. Unless otherwise stated, the simulation parameters for the network are provided in Table I. The Monte Carlo simulations construct the meta distribution $\bar{F}_s(\theta_n, \delta)$ across 5000 different HPF realizations with 10^5 time iterations per each HPF realization. For the analysis, the feedback success probability p_{ack} is obtained

TABLE I: Network and simulation parameters

Symbol	Definition	Value
λ	Intensity of PPP Ψ	2×10^2 devices/Km ²
η	Fading exponent	4
R_o	Distance of Tx/Rx link	20 meters
\mathcal{V}	Types of IoT interfering devices	3
$f_{v(v)}$	PMF of types of IoT interfering devices	Uniform
α_v	Activity of type v IoT interfering devices	{0.1, 0.3, 0.5}
p_v	Transmitted power of type v IoT interfering devices	{10, 7, 5} mWatts
p_t	Transmitted power of the test IoT device	10 mWatt
W	Bandwidth	250 KHz
L	Packet length	300 Bytes
T_s	Packet duration	1 ms
T	Packet deadline	15 time slots
p_{ct}	Tx mode RF circuit power consumption	38 mWatt [45]
p_{cr}	Rx mode RF circuit power consumption	45 mWatt [45]
γ	Power amplifier conversion factor	4 [44]
L_{ack}	ACK/NACK messages length	{5, 15} Bytes
T_{ack}	ACK/NACK messages duration	$0.15 T_s = 0.15$ ms

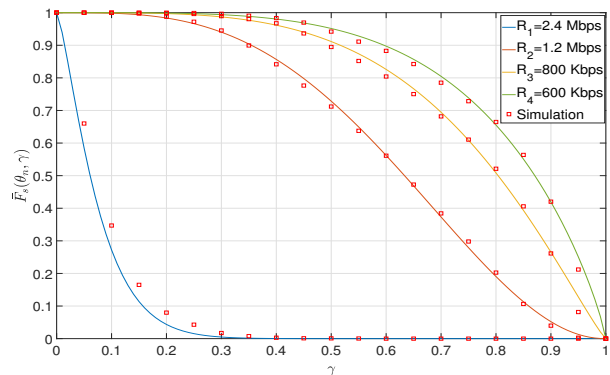


Fig. 4: Meta distribution of the FSD at different transmission rates R_n , $n \in \{1, \dots, 4\}$.

in (20). The meta distribution of the FSD probability for each rate R_n is obtained as in (14). The transition matrices of the CLRA and OLRA schemes defined, respectively, in Lemmas 1 and 2 are constructed upon obtaining the FSD probability $p_{n,m}$, $m = \{1, 2, \dots, M\}$ from (18), which discretizes the FSD meta distribution in (14). By relying on the constructed matrices, the performance metrics of a generic IoT device (i.e., PSD probability, PSD mean latency and overall energy consumption) are obtained in Theorem 1, Corollary 1, and Corollary 2.

Fig. 4 shows the meta distribution of the FSD for different transmission rates. The close match between the analysis (i.e., curves) and simulations (marks) validates the beta distribution approximation of the meta distribution used in (14). The figure also shows the impact of transmission rate R_n on the FSD probability (i.e., transmission reliability). Dividing the packet into more fragments enables a lower transmission rate and leads to a lower detection threshold θ_n that is more likely to be satisfied, which improves the transmission reliability. For instance, dividing the packet into 2 fragments significantly improves the probability that the SIR decoding threshold θ_n is satisfied by the intended link for 20% percent of the time from 0.04 to 0.98.

Before comparing the CLRA and OLRA schemes to quantify the impact of feedback, we first contrast the two OLRA variants in Fig. 5. In particular, Fig. 5 depicts the PSD probability and mean latency of the proposed OLRA and OLRA-ES transmission schemes. At first, we highlight the match between the analysis and simulation results, which

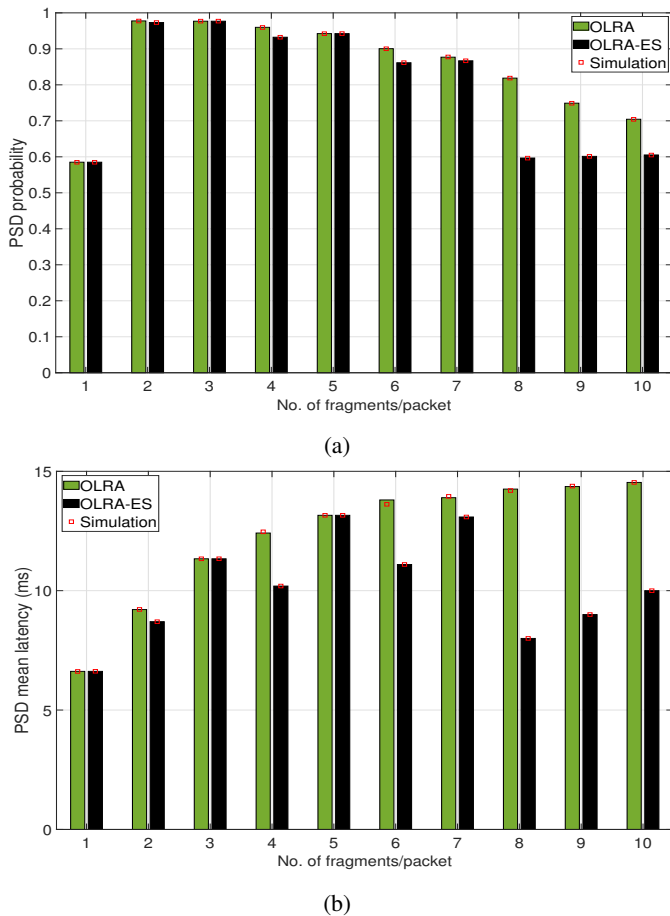


Fig. 5: PSD probability and mean latency for OLRA transmission schemes.

validates our developed mathematical framework. Recalling from Section IV-A2, both schemes have a minimum repetition of $\kappa = \lfloor T/n \rfloor$ times for each fragment. However, both schemes differ in the way they exploit the remaining $\tau = \text{mod}(T, n)$ time slots. Fig. 5 confirms that both schemes have similar performance when T is divisible by n (i.e., the number of remaining slots τ is 0) shown for the cases of $n \in \{1, 3, 5\}$. For other values of n , the figure illustrates that OLRA outperforms OLRA-ES in terms of transmission reliability, at the expense of increased transmission latency, as depicted in Fig. 5b. This disparity arises from the transmission of τ fragments from the n fragments $\kappa + 1$ times in the OLRA scheme, compared to the κ times in the OLRA-ES scheme. The superiority of OLRA over OLRA-ES in transmission reliability is governed by the values of κ and τ . A higher value of κ increases the likelihood of successful fragment delivery within κ decoding trials, diminishing the significance of sending τ fragments an additional time, resulting in a less pronounced improvement in PSD probability. For instance, for $n = 4$ (i.e., $\kappa = 3$ and $\tau = 3$), the PSD probability of OLRA surpasses that of the OLRA-ES scheme by 3%, with a 22.8% increase in latency. Conversely, a smaller κ signifies the impact of τ on the transmission reliability at the expense of latency increment. For instance, with $n = 8$ (i.e., $\kappa = 1$ and $\tau = 7$), the PSD probability escalates by 37.2%, at the cost of a 78.3% latency increment.

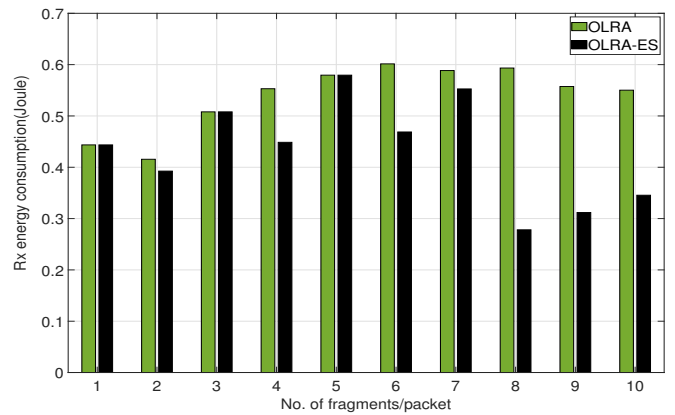


Fig. 6: Receiver energy consumption for OLRA schemes.

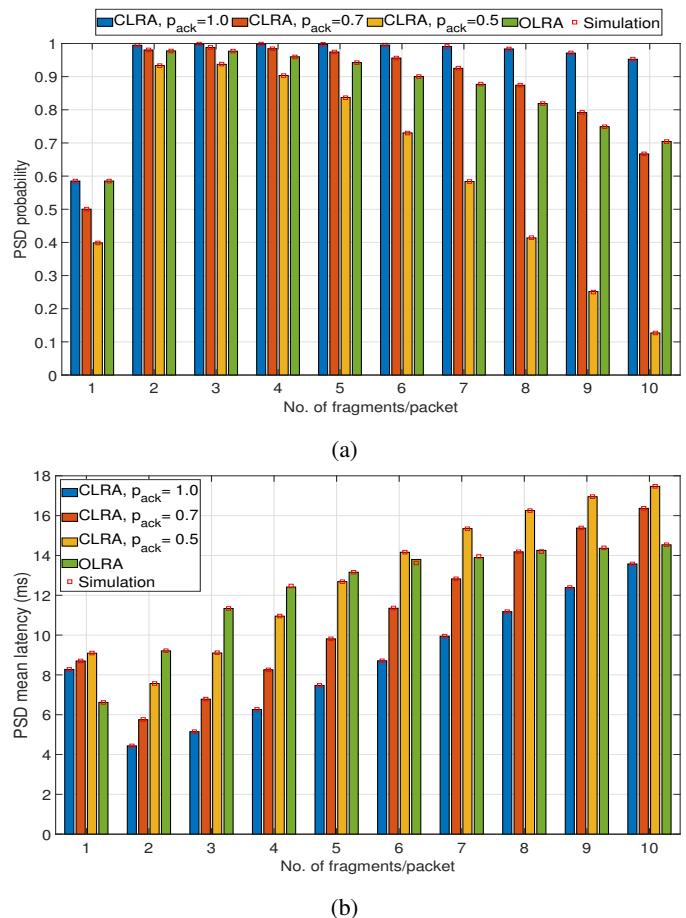


Fig. 7: Comparison between OLRA and CLRA schemes in terms of PSD probability and mean latency.

Fig. 6 illustrates the energy consumption of the test receiver when decoding a standard packet from the corresponding transmitter in both the OLRA and OLRA-ES schemes. We can clearly see that the OLRA consumes more energy due to its increased PSD latency compared to the OLRA-ES scheme, as shown in Fig. 5b. This observation aligns with the relationship described in (26). Since the OLRA is superior to its OLRA-ES counterpart, we use the former to quantify the impact of the feedback by benchmarking against the CLRA scheme. In this context, Fig. 7 compares the OLRA with the feedback-aware CLRA scheme for three values of p_{ack} .

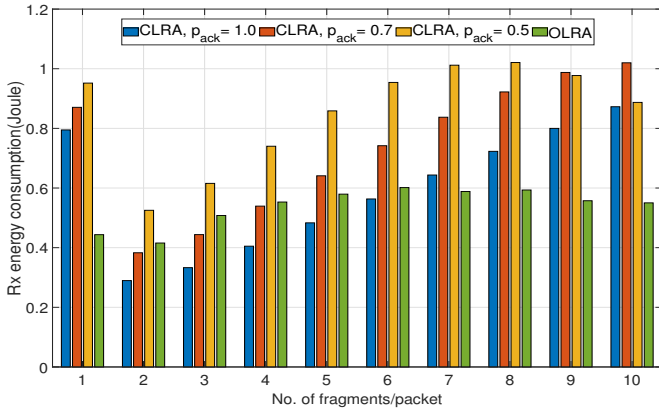


Fig. 8: Comparison between OLRA and CLRA schemes in terms of receiver energy consumption in packet decoding.

The $p_{\text{ack}} = 1$ represents the idealistic error-free feedback channel that shows the best performance in terms of reliability and latency. Accounting for the feedback errors reveals the true performance, which can be significantly less than the idealistic case as shown for $p_{\text{ack}} = 0.7$ (i.e., $L_{\text{ack}} = 5$ Bytes) and $p_{\text{ack}} = 0.5$ (i.e., $L_{\text{ack}} = 15$ Bytes). The impact of the feedback is quantified by comparing the feedback-free OLRA to the CLRA scheme. It can be shown that the CLRA scheme outperforms OLRA by 2.5% when the number of fragments $n = 4$ and $p_{\text{ack}} = 0.7$. The figure also shows that the OLRA scheme has a higher transmission latency. However, for higher feedback errors, the OLRA-FR scheme performs better in terms of reliability and latency. In all schemes, the positive impact of packet fragmentation is underscored showing an optimal number of fragments that maximizes the reliability. The PSD probability for $n > 1$ (i.e., with fragmentation) is remarkably higher than for $n = 1$ (i.e., without fragmentation) at the expense of increased transmission latency.

Although the CLRA scheme can improve transmission reliability, it has a direct impact on the energy consumption of IoT devices. Fig. 8 highlights the cost of the feedback-aware CLRA scheme over the feedback-free OLRA scheme in terms of the overall energy consumption by the test receiver in packet reception and decoding and feedback ACK/NACK transmissions. It can be clearly shown that the receiver adopting the CLRA transmission scheme consumes more energy compared with the OLRA scheme owing to the energy consumed in the feedback transmission. Furthermore, Fig. 8 shows the negative impact of feedback channel imperfection on the receiver energy consumption for the CLRA scheme.

VI. CONCLUSION

In this paper, feedback-aware CLRA and feedback-free OLRA transmission schemes tailored for delay-sensitive and energy-constrained large-scale IoT networks are addressed. Novel and tractable spatiotemporal frameworks based on stochastic geometry and queuing theory are developed for the OLRA transmission schemes and benchmarked against the CLRA scheme under an error-prone feedback setting. The simulation outcomes validate the analytical models for both OLRA and CLRA and emphasize a crucial insight that rate adaptation substantially improves transmission reliability, at

the expense of latency. Notably, our findings underscore the adverse effects of imperfections within the feedback channel on the CLRA scheme, manifested in reduced reliability and increased energy consumption. Furthermore, our results quantify the energy savings achieved by the feedback-free OLRA scheme and reveal the tradeoff in terms of transmission reliability and latency when compared to the error-prone feedback-aware CLRA scheme. In essence, the results quantify the energy saving of the feedback-free OLRA scheme at the expense of transmission reliability reduction and latency increment compared with the feedback-aware CLRA scheme.

APPENDIX A PROOF OF LEMMA 4

The first and second moments of the FSD probability p_n , i.e., M_1 and M_2 can be obtained by averaging p_n in (13) over the devices types, activities, fading gains, and the spatial locations of the devices. Hence, M_1 is given by

$$\begin{aligned}
 M_1 &= \mathbb{E}_{h_o, \xi_i, g_i, \Psi} \left\{ \frac{p_o h_o R_o^{-\eta}}{\sum_{v=1}^V \sum_{x_i \in \Psi_v \setminus x_o} \mathbb{1}_{\xi_i} p_v g_i R_i^{-\eta}} \geq \theta_n \right\} \\
 &\stackrel{(a)}{=} \mathbb{E}_{\xi_i, g_i, \Psi} \left\{ \exp \left[-\theta_n \sum_{v=1}^V \sum_{x_i \in \Psi_v \setminus x_o} \mathbb{1}_{\xi_i} \frac{p_v g_i R_o^\eta}{p_o R_i^\eta} \right] \right\} \\
 &\stackrel{(b)}{=} \mathbb{E}_{\Psi} \left\{ \prod_{v=1}^V \prod_{x_i \in \Psi_v \setminus x_o} \frac{\alpha_v}{1 + \frac{\theta_n p_v R_o^\eta}{p_o R_i^\eta}} + (1 - \alpha_v) \right\} \\
 &\stackrel{(c)}{=} \exp \left[-2\pi \sum_{v=1}^V \lambda_v \int_0^\infty \left(1 - \left(1 - \frac{\alpha_v \frac{\theta_n p_v R_o^\eta}{p_o x^\eta}}{1 + \frac{\theta_n p_v R_o^\eta}{p_o x^\eta}} \right) \right) x dx \right] \\
 &\stackrel{(d)}{=} \exp \left[\frac{-2\pi R_o^2 \theta_n^{2/\eta}}{\eta} \sum_{v=1}^V \left(\frac{p_v}{p_o} \right)^{\frac{2}{\eta}} \lambda_v \alpha_v \int_0^\infty \frac{y^{-\frac{2}{\eta}}}{1+y} dy \right],
 \end{aligned}$$

where (a) follows from the exponentially-distributed power gain of the intended channel (i.e., $h_o \sim \exp(1)$); (b) follows from the Bernoulli distribution of the IoT interfering device activity indicator $\mathbb{1}_{\xi_i}$ and $g_i \sim \exp(1)$; (c) follows from the probability generating functional (PGFL) of the PPP [46]; (d) is obtained by changing variables $y = \frac{\theta_n p_v R_o^\eta}{p_o x^\eta}$. By manipulating the integral in (d), M_1 in (15) is obtained.

Similarly, the second moment of the FSD probability M_2 can be obtained as follows

$$\begin{aligned}
 M_2 &= \mathbb{E}_{\Psi} \left[\prod_{v=1}^V \prod_{x_i \in \Psi_v \setminus x_o} \left(\frac{\alpha_v}{1 + \frac{\theta_n p_v R_o^\eta}{p_o R_i^\eta}} + (1 - \alpha_v) \right)^2 \right] \\
 &= \exp \left[-2\pi \sum_{v=1}^V \lambda_v \left\{ 2\alpha_v \int_{x=0}^\infty \frac{\left(\frac{\theta_n p_v R_o^\eta}{p_o x^\eta} \right)}{\left(1 + \frac{\theta_n p_v R_o^\eta}{p_o x^\eta} \right)} x dx \right. \right. \\
 &\quad \left. \left. - \alpha_v^2 \int_{x=0}^\infty \frac{\left(\frac{\theta_n p_v R_o^\eta}{p_o x^\eta} \right)^2}{\left(1 + \frac{\theta_n p_v R_o^\eta}{p_o x^\eta} \right)^2} x dx \right\} \right],
 \end{aligned}$$

By manipulating the integrals in a similar way to (15), the expression of M_2 is obtained as provided in Lemma 3.

REFERENCES

- [1] L. Zhang, Y.-C. Liang, and D. Niyato, "6G visions: Mobile ultra-broadband, super internet-of-things, and artificial intelligence," *China Communications*, vol. 16, no. 8, pp. 1–14, 2019.
- [2] W. Saad, M. Bennis, and M. Chen, "A vision of 6G wireless systems: Applications, trends, technologies, and open research problems," *IEEE network*, vol. 34, no. 3, pp. 134–142, 2019.
- [3] Ericsson, "Ericsson Mobility Report." [Online]. Available: <https://www.ericsson.com/assets/local/reports-papers/mobility-report/documents/2020/november-2020-ericsson-mobility-report.pdf>
- [4] M. Bennis, M. Debbah, and H. V. Poor, "Ultrareliable and low-latency wireless communication: Tail, risk, and scale," *Proceedings of the IEEE*, vol. 106, no. 10, pp. 1834–1853, 2018.
- [5] R. Jurdi, S. R. Khosravirad, H. Viswanathan, J. G. Andrews, and R. W. Heath, "Outage of periodic downlink wireless networks with hard deadlines," *IEEE Transactions on Communications*, vol. 67, no. 2, pp. 1238–1253, 2018.
- [6] W. Tang, R. Zhang, and S. Feng, "A spatiotemporal model for hard-deadline multistream traffic in uplink IoT networks," *IEEE Internet of Things Journal*, vol. 9, no. 1, pp. 601–615, 2021.
- [7] O. Liberg, M. Sundberg, E. Wang, J. Bergman, and J. Sachs, *Cellular Internet of things: technologies, standards, and performance*. Academic Press, 2017.
- [8] A. Yegin, T. Kramp, P. Dufour, R. Gupta, R. Soss, O. Hersent, D. Hunt, and N. Sornin, "Lorawan protocol: specifications, security, and capabilities," in *LPWAN Technologies for iot and m2m applications*. Elsevier, 2020, pp. 37–63.
- [9] S. Aguilar, R. Vidal, and C. Gomez, "Evaluation of receiver-feedback techniques for fragmentation over lpwans," *IEEE Internet of Things Journal*, vol. 9, no. 9, pp. 6866–6878, 2021.
- [10] H. ElSawy, "Rate adaptation and latency in heterogeneous IoT networks," *IEEE Communications Letters*, vol. 25, no. 2, pp. 660–664, 2020.
- [11] Y. Nabil, H. ElSawy, S. Al-Dharrab, H. Mostafa, and H. Attia, "Data aggregation in regular large-scale IoT networks: Granularity, reliability, and delay tradeoffs," *IEEE Internet of Things Journal*, vol. 9, no. 18, pp. 17767–17784, 2022.
- [12] Z. Zhao, G. Min, W. Gao, Y. Wu, H. Duan, and Q. Ni, "Deploying edge computing nodes for large-scale IoT: A diversity aware approach," *IEEE Internet of Things Journal*, vol. 5, no. 5, pp. 3606–3614, 2018.
- [13] M. Masoudi, A. Azari, E. A. Yavuz, and C. Cavdar, "Grant-free radio access IoT networks: Scalability analysis in coexistence scenarios," in *IEEE International Conference on Communications (ICC)*, 2018, pp. 1–7.
- [14] K. Huang, W. Liu, Y. Li, A. Savkin, and B. Vucetic, "Wireless feedback control with variable packet length for industrial IoT," *IEEE Wireless Communications Letters*, vol. 9, no. 9, pp. 1586–1590, 2020.
- [15] C. Yu, L. Yu, Y. Wu, Y. He, and Q. Lu, "Uplink scheduling and link adaptation for narrowband internet of things systems," *IEEE Access*, vol. 5, pp. 1724–1734, 2017.
- [16] C. Zheng, F.-C. Zheng, J. Luo, and D. Feng, "Open-loop communications for up-link urllc under clustered user distribution," *IEEE Transactions on Vehicular Technology*, vol. 70, no. 11, pp. 11509–11522, 2021.
- [17] H. Khodr, N. Kouzayha, M. Abdallah, J. Costantine, and Z. Dawy, "Energy efficient IoT sensor with RF wake-up and addressing capability," *IEEE sensors letters*, vol. 1, no. 6, pp. 1–4, 2017.
- [18] N. Kouzayha, Z. Dawy, J. G. Andrews, and H. ElSawy, "Joint downlink/uplink RF wake-up solution for IoT over cellular networks," *IEEE Transactions on Wireless Communications*, vol. 17, no. 3, pp. 1574–1588, 2017.
- [19] H. ElSawy, A. Sultan-Salem, M.-S. Alouini, and M. Z. Win, "Modeling and analysis of cellular networks using stochastic geometry: A tutorial," *IEEE Communications Surveys & Tutorials*, vol. 19, no. 1, pp. 167–203, 2016.
- [20] A. Bader, H. ElSawy, M. Gharbieh, M.-S. Alouini, A. Adinoyi, and F. Alshalan, "First mile challenges for large-scale IoT," *IEEE Communications Magazine*, vol. 55, no. 3, pp. 138–144, 2017.
- [21] F. Benkhelifa, H. ElSawy, J. A. Mccann, and M.-S. Alouini, "Recycling cellular energy for self-sustainable IoT networks: A spatiotemporal study," *IEEE Transactions on Wireless Communications*, vol. 19, no. 4, pp. 2699–2712, 2020.
- [22] M. A. Abd-Elmagid, M. A. Kishk, and H. S. Dhillon, "Joint energy and SINR coverage in spatially clustered RF-powered IoT network," *IEEE Transactions on Green Communications and Networking*, vol. 3, no. 1, pp. 132–146, 2018.
- [23] M. Emara, H. ElSawy, and G. Bauch, "Prioritized multistream traffic in uplink IoT networks: Spatially interacting vacation queues," *IEEE internet of things journal*, vol. 8, no. 3, pp. 1477–1491, 2020.
- [24] Y. Zhong, T. Q. Quek, and X. Ge, "Heterogeneous cellular networks with spatio-temporal traffic: Delay analysis and scheduling," *IEEE Journal on Selected Areas in Communications*, vol. 35, no. 6, pp. 1373–1386, 2017.
- [25] M. Gharbieh, H. ElSawy, A. Bader, and M.-S. Alouini, "Spatiotemporal stochastic modeling of IoT enabled cellular networks: Scalability and stability analysis," *IEEE Transactions on Communications*, vol. 65, no. 8, pp. 3585–3600, 2017.
- [26] Q. Zhang, H. H. Yang, T. Q. Quek, and S. Jin, "Spatiotemporal modeling of massive MIMO systems with mixed-type IoT devices: Scheduling optimization with delay constraints," *IEEE Internet of Things Journal*, vol. 8, no. 12, pp. 10146–10159, 2021.
- [27] M. Gharbieh, H. ElSawy, H.-C. Yang, A. Bader, and M.-S. Alouini, "Spatiotemporal model for uplink IoT traffic: Scheduling and random access paradox," *IEEE Transactions on Wireless Communications*, vol. 17, no. 12, pp. 8357–8372, 2018.
- [28] N. Jiang, Y. Deng, A. Nallanathan, X. Kang, and T. Q. Quek, "Analyzing random access collisions in massive IoT networks," *IEEE Transactions on Wireless Communications*, vol. 17, no. 10, pp. 6853–6870, 2018.
- [29] G. Chisci, H. ElSawy, A. Conti, M.-S. Alouini, and M. Z. Win, "Uncoordinated massive wireless networks: Spatiotemporal models and multiaccess strategies," *IEEE/ACM Transactions on Networking*, vol. 27, no. 3, pp. 918–931, 2019.
- [30] H. G. Moussa and W. Zhuang, "RACH performance analysis for large-scale cellular IoT applications," *IEEE Internet of Things Journal*, vol. 6, no. 2, pp. 3364–3372, 2018.
- [31] H. H. Yang and T. Q. Quek, "Spatiotemporal analysis for SINR coverage in small cell networks," *IEEE Transactions on Communications*, vol. 67, no. 8, pp. 5520–5531, 2019.
- [32] H. H. Yang, Y. Wang, and T. Q. Quek, "Delay analysis of random scheduling and round robin in small cell networks," *IEEE Wireless Communications Letters*, vol. 7, no. 6, pp. 978–981, 2018.
- [33] H. ElSawy, "Characterizing IoT networks with asynchronous time-sensitive periodic traffic," *IEEE Wireless Communications Letters*, vol. 9, no. 10, pp. 1696–1700, 2020.
- [34] J. Li, Y. Zhou, and H. Chen, "Age of information for multicast transmission with fixed and random deadlines in IoT systems," *IEEE Internet of Things Journal*, vol. 7, no. 9, pp. 8178–8191, 2020.
- [35] C. She, C. Yang, and T. Q. Quek, "Cross-layer optimization for ultra-reliable and low-latency radio access networks," *IEEE Transactions on Wireless Communications*, vol. 17, no. 1, pp. 127–141, 2017.
- [36] M. Wu, Y. Zhong, G. Wang, C. She, X. Ge, and H.-C. Chao, "URLLC in large-scale wireless networks with time and frequency diversities," in *IEEE Global Communications Conference (GLOBECOM)*, 2019, pp. 1–6.
- [37] B. Manzoor, B. Al Homssi, and A. Al-Hourani, "IoT coverage enhancement using repetition in energy constrained devices: An analytic approach," *IEEE Transactions on Green Communications and Networking*, vol. 6, no. 2, pp. 1122–1131, 2021.
- [38] B. Manzoor, B. Al Homssi, A. Al-Hourani, and S. Kandeepan, "Optimal repetition rate for maximal coverage," *IEEE Wireless Communications Letters*, vol. 10, no. 4, pp. 800–804, 2020.
- [39] B. Manzoor, A. Al-Hourani, and B. Al Homssi, "Improving IoT-over-satellite connectivity using frame repetition technique," *IEEE Wireless Communications Letters*, vol. 11, no. 4, pp. 736–740, 2022.
- [40] S. Rezasoltani and C. Assi, "Real-time status updates in wireless harq with imperfect feedback channel," *IEEE Transactions on Wireless Communications*, vol. 21, no. 6, pp. 4212–4226, 2021.
- [41] A. S. Alfa, *Applied discrete-time queues*. Springer, 2016.
- [42] M. Haenggi, "The meta distribution of the SIR in poisson bipolar and cellular networks," *IEEE Transactions on Wireless Communications*, vol. 15, no. 4, pp. 2577–2589, 2015.
- [43] O. Amin, S. Bavarian, L. Lampe, E. Hossain, V. K. Bhargava, and G. P. Fettweis, "Cooperative techniques for energy-efficient wireless communications," *Green radio communication networks*, vol. 2020, pp. 125–151, 2012.
- [44] B. Al Homssi, A. Al-Hourani, S. Chandrasekharan, K. M. Gomez, and S. Kandeepan, "On the bound of energy consumption in cellular IoT networks," *IEEE Transactions on Green Communications and Networking*, vol. 4, no. 2, pp. 355–364, 2019.
- [45] N. Semiconductor, "nRF24L01 datasheet," *Single Chip*, vol. 2, 2009.
- [46] M. Haenggi, *Stochastic geometry for wireless networks*. Cambridge University Press, 2012.